THE JOURNAL OF BIOLOGICAL CHEMISTRY
Vol. 277, No. 39, Issue of September 27, pp. 36321–36328, 2002
Printed in U.S.A.

Specific Orientation and Two-dimensional Crystallization of the Proteasome at Metal-chelating Lipid Interfaces*

Received for publication, March 5, 2002, and in revised form, July 4, 2002
Published, JBC Papers in Press, July 11, 2002, DOI 10.1074/jbc.M202145200

Andreas Thess‡§, Silke Hutschenreiter¶, Matthias Hofmann‡, Robert Tampé¶, Wolfgang Baumeister‡, and Reinhard Guckenberger‡‖

From the ‡Abteilung Molekulare Strukturbiologie, Max-Planck-Institut für Biochemie, 82152 Martinsried, Germany and the ¶Institut für Biochemie, Biozentrum, Goethe-Universität Frankfurt, Marie-Curie-Str. 9, 60439 Frankfurt a.M., Germany

The potential of a protein-engineered His tag to immobilize macromolecules in a predictable orientation at metal-chelating lipid interfaces was investigated using recombinant 20 S proteasomes His-tagged in various positions. Electron micrographs demonstrated that the orientation of proteasomes bound to chelating lipid films could be controlled via the location of their His tags: proteasomes His-tagged at their sides displayed exclusively side-on views, while proteasomes His-tagged at their ends displayed exclusively end-on views. The activity of proteasomes immobilized at chelating lipid interfaces was well preserved. In solution, His-tagged proteasomes hydrolyzed casein at rates comparable with wild-type proteasomes, unless the His tags were located in the vicinity of the N termini of α-subunits. The N termini of α-subunits might partly occlude the entrance channel in α-rings through which substrates enter the proteasome for subsequent degradation. A combination of electron micrographs and atomic force microscope topographs revealed a propensity of vertically oriented proteasomes to crystallize in two dimensions on fluid lipid films. The oriented immobilization of His-tagged proteins at biocompatible lipid interfaces will assist structural studies as well as the investigation of biomolecular interaction via a wide variety of surface-sensitive techniques including single-molecule analysis.

Structural and functional studies of biological molecules are often based on surface-sensitive techniques, among them attenuated total reflection infrared spectroscopy, evanescent field fluorescence microscopy, ellipsometry, and scanning probe microscopies. Hence, a wide range of techniques would benefit from a generally applicable approach to the immobilization of biological macromolecules. As a key requirement, any general strategy to immobilization will have to fully preserve the biological activity of molecules subjected to it; any adverse effects that immobilization might have on molecules in terms of their structure and function should be minimized. The sites relevant to their biological function like ligand-binding sites or active sites must remain accessible after transfer to a solid surface. This demands that the orientation of the molecule with respect to the supporting interface can be fully controlled.

Formation of metal-chelate complexes is a strategy commonly used for the purification of proteins containing an engineered His tag, *i.e.* a stretch of consecutive histidines (1). Nitrilotriacetic acid (NTA)[1] binds nickel ions coordinatively (2), leaving two coordination sites available for interaction with a His tag. Binding of His-tagged proteins to a Ni-NTA presenting surface is specific (3) with a binding constant in the micromolar range (4), but easily reversible. Importantly, via judicious introduction of a His tag, the site through which molecules bind to a chelating support and, possibly, their orientation with respect to a chelating support, can be controlled.

The 20 S proteasome is a large multisubunit protease, which plays a key role in the degradation of misfolded proteins and of short-lived regulatory proteins (5–7). Its 28 subunits are arranged in four heptameric rings, which collectively form a barrel-shaped complex 15 nm in length and 11 nm in diameter. There are two types of subunits, α and β; the α-type subunits form the two outer rings and the β-type subunits the two inner rings. In most prokaryotes, including the *Archaeon Thermoplasma acidophilum*, the rings are homoheptameric; thus, the stoichiometry of these 20 S proteasomes is $\alpha_7\beta_7\beta_7\alpha_7$ (Fig. 1*A*).

Proteasomes are members of the superfamily of Ntn (N-terminal nucleophile) hydrolases; a common feature of this group of enzymes is a single-residue active site, *i.e.* both the nucleophile and the primary proton acceptor are provided by the same N-terminal residue. In the proteasome this is the Thr^1 of the β-subunits (8, 9). During assembly, 20 S proteasomes undergo a post-translational modification that removes a propeptide and exposes the α-amino group of Thr^1 (10). In mature 20 S proteasomes Thr^1 is accessible only from the central, ~5 nm wide cavity, which is formed by the two rings of β-subunits (Fig. 1*A*). Substrates destined for degradation must therefore be translocated into the interior of the proteasome from either end through entrance channels situated at the center of the two α-rings (11) (Fig. 1*A*). Turn forming segments around Tyr^{126} of the seven α-subunits appear to define the properties of these 1.3-nm wide channels, although it should be noted that there are several disordered residues (8) that are likely to (partially) occlude the channels. In any case, access to the interior of the proteasome and thus to the active sites is restricted to completely unfolded polypeptide chains (11).

* This work was supported by the Volkswagenstiftung. The costs of publication of this article were defrayed in part by the payment of page charges. This article must therefore be hereby marked "*advertisement*" in accordance with 18 U.S.C. Section 1734 solely to indicate this fact.

§ Supported by a postdoctoral fellowship of the Deutsche Forschungsgemeinschaft. Present address: m-phasys GmbH, Vor dem Kreuzberg 17, 72070 Tübingen, Germany.

‖ To whom correspondence should be addressed. Tel.: 49-89-8578-2651; Fax: 49-89-8578-2641; E-mail: guckenbe@biochem.mpg.de.

[1] The abbreviations used are: NTA, nitrilotriacetic acid; Ni-NTA, nickel-nitrilotriacetic acid; DODA, N^{α},N^{α}-bis(carboxymethyl)-N^{ϵ}-[(dioctadecylamino)-succinyl]-L-lysine; SOPC, 1-stearoyl-2-oleoyl-*sn*-glycero-3-phosphatidylcholine; DSPC, 1,2-distearoyl-*sn*-glycero-3-phosphatidylcholine; AFM, atomic force microscope; Suc-LLVY-AMC, succinyl-Leu-Leu-Val-Tyr-7-amido-4-methylcoumarin.

Therefore, to be functional *in vivo*, 20 S proteasomes must associate with regulatory complexes, invariably containing AAA-ATPases, which prepare substrates for degradation by unfolding them (12–14). Moreover, regulatory complexes such as the 19 S caps of eukaryotic proteasomes have been implicated in gating the α-ring channels (15, 16).

To explore the use of a His tag as a handle that might allow one to immobilize functional molecules in a predictable orientation, we have generated recombinant 20 S proteasomes His-tagged in various positions. The option to immobilize proteasomes in a uniform and predetermined orientation allowing regulatory complexes unhindered binding holds prospect for structural studies addressing the interaction of the proteasome with cofactors and their role in substrate translocation. Immobilizing proteasomes while fully preserving their proteolytic activity will benefit investigations of proteasome-substrate interaction in real time for detailed kinetic analysis, possibly at the single molecule level. Following biochemical characterization of His-tagged proteasomes, their interaction with metal-chelating lipid interfaces has been assessed.

EXPERIMENTAL PROCEDURES

Materials—PFU-TURBO polymerase from Stratagene (Amsterdam, The Netherlands) in combination with dNTPs (polymerization mixture) from Amersham Biosciences were used in polymerase chain reactions. Sequencing was performed using the BIGDYE terminator cycle sequencing kit from PerkinElmer Life Sciences. 20 S proteasomes were purified either on Ni-NTA resin (SUPERFLOW from Qiagen GmbH, Hilden, Germany) or hydroxyapatite (Bio-Gel HTP from Bio-Rad). Bicinchoninic acid solution was from Sigma. Protease activity was assayed using succinyl-Leu-Leu-Val-Tyr-7-amido-4-methylcoumarin (Suc-LLVY-AMC) from Bachem (Heidelberg, Germany) or ^{14}C-methylated β-casein from Sigma. Mica was glued to Teflon sheets with Bindulin two-component epoxy glue (Fürth, Germany). The chelating lipid NTA-DODA (N^{α},N^{α}-bis(carboxymethyl)-N^{ϵ}-[(dioctadecylamino)-succinyl]-L-lysine) was synthesized as described (17). SOPC (1-stearoyl-2-oleoyl-*sn*-glycero-3-phosphatidylcholine) was from Avanti Polar Lipids, whereas DSPC (1,2-distearoyl-*sn*-glycero-3-phosphatidylcholine) was from Sigma.

Mutagenesis, Expression, and Purification of 20 S Proteasomes—pRSET6a plasmids coding for both the α-subunit and β-subunit (either wild-type or His-tagged at the C terminus) of the 20 S proteasome from *T. acidophilum* (referred to simply as "proteasome" in the following) were provided by Dr. Erika Seemüller. His tags were introduced into the α-subunit starting from the plasmid coding for the wild-type proteasome using whole plasmid amplification via the polymerase chain reaction (Pfu-turbo polymerase) starting with primers including the desired changes. Sequencing was performed on a PerkinElmer Life Sciences applied biosystems 373 DNA sequencer. The α- and β-subunits of the proteasome were coexpressed in *Escherichia coli* BL21(DE3). The assembled complex was purified either on Ni-NTA resin or on hydroxyapatite if the affinity for Ni-NTA resin was low. In the latter case, material bound to hydroxyapatite was eluted with a gradient from 10 to 600 mM potassium phosphate buffer, pH 7; proteasomes eluted at around 500–550 mM potassium phosphate. Purity of fractions showing proteasomal activity against Suc-LLVY-AMC was tested by SDS-polyacrylamide gel electrophoresis. Protein concentration was determined using the bicinchoninic acid assay.

Activity of Proteasomes in Solution—To follow the degradation of fluorogenic substrates in solution, Suc-LLVY-AMC was dissolved at 10 mM in dimethyl sulfoxide (Me_2SO) and added at a final concentration of 125 μM (1.25% Me_2SO) in 800 μl of buffer A (50 mM Tris, pH 7.5) containing 100 ng of proteasomes (corresponding to 0.18 nM) for continuous measurement at 60 °C. The released AMC was detected ($\lambda_{ex/em}$ 380 nm/440 nm) in an LS 50 B fluorescence spectrometer (PerkinElmer Life Sciences).

To follow the degradation of proteins in solution, 11 μg of ^{14}C-methylated β-casein (21,800 cpm/μg, final concentration 8.76 μM) was digested with 300–600 ng of proteasomes (8.6–17.2 nM) in 50 μl of buffer A for 40 min at 60 °C. The reaction was stopped by adding 1 ml of 12% trichloroacetic acid followed by incubation on ice for 30 min. Centrifugation for 20 min in the presence of 10 μl of bovine serum albumin (1%) at 13,000 $\times$ *g* separated acid-soluble degradation products that were quantified in a TRI CARB 1500 liquid scintillation counter (Packard Instrument Co.).

Preparation of Vesicles and Supported Nickel-chelating Lipid Bilayers—For preparation of lipid vesicles, NTA-DODA and SOPC were mixed (1:9 mol/mol) in chloroform. NTA-DODA was loaded with nickel ions (Ni-NTA-DODA) in chloroform/methanol (3:1) by adding equimolar amounts of $NiCl_2 \cdot 6H_2O$ dissolved in methanol. After evaporation of the solvent under a stream of nitrogen, vesicles were obtained by swelling in buffer B (10 mM Hepes, 150 mM NaCl, pH 7.5) to a final lipid concentration of 2 mM and repeated extrusion (30 times) through 100-nm filters (LIPOSO FAST-BASIC, Avestin, Ottawa, Canada).

Supported lipid bilayers were prepared on mica sheets glued to Teflon supports cut to either fit quartz cuvettes (3 mm $\times$ 9 mm) or the fluid cell of an atomic force microscope (6 mm diameter). Freshly cleaved mica was first incubated with buffer B containing 15 mM Mg^{2+} for 60 min, then with vesicle solution (Ni-NTA-DODA/SOPC, 1:9) at 50 °C to yield bilayers. Preincubation of mica with Mg^{2+} resulted in increased bilayer stability; presumably Mg^{2+} is required to compensate for the negative surface charge of both mica and chelating lipid film. After 3 h, the surfaces were thoroughly rinsed with buffer B.

Activity of Proteasomes Immobilized at Nickel-chelating Lipid Interfaces—The activity of proteasomes was tested after immobilization on two kinds of bilayer specimens, that is on vesicle bilayers and on mica supported bilayers. For the first set of measurements, vesicles were prepared as described in the previous section. 11 nM proteasomes were incubated with these vesicles at a proteasome/chelator lipid ratio of 1:910 for 3 h at 4 °C. Degradation of 125 μM Suc-LLVY-AMC by the proteasomes immobilized on the vesicles was performed for 15 min at 60 °C. The reaction was stopped by addition of a 9-fold excess of 100 mM chloroacetic acid, 100 mM acetic acid, pH 4.3, before quantifying fluorescence. The activity of unbound proteasomes was measured in the presence of 250 mM imidazole, which leads to desorption of the proteasomes from the Ni-chelator lipid.

For the measurements with proteasomes bound to solid supported bilayers, first the activity of a known amount of proteasomes in solution was assayed. Quartz cuvettes holding 300 ng of proteasomes in 2970 μl of buffer C (100 mM Tris, pH 7.5) were equilibrated at 40 °C for 15 min. Following addition of 30 μl of Suc-LLVY-AMC (final concentration 100 μM Suc-LLVY-AMC, 1% Me_2SO, 0.14 nM proteasome), cuvettes were kept at 40 °C for 30 min, then chilled on ice for 5 min. Released AMC was detected ($\lambda_{ex/em}$ 380 nm/440 nm) in a fluorescence spectrometer.

An equal amount of His-tagged proteasomes (300 ng) was adsorbed onto a mica-supported nickel-chelating lipid bilayer (Ni-NTA-DODA/SOPC, 1:9) overnight to allow them to bind. Proteasomes that did not bind were transferred using a pipette into a cuvette holding 2970 μl of buffer C. The rate at which AMC was released by the unbound proteasomes was quantified as before. Subtracting this rate from the rate at which 300 ng of proteasomes in solution released AMC equals the rate at which those proteasomes bound to the bilayer would release AMC if their activity was not affected by immobilization at all (the "ideal rate"). The rate at which proteasomes immobilized on the supported bilayer overnight actually released AMC was measured as before after placing the mica-supported bilayer with bound proteasomes at the bottom of a cuvette holding 2970 μl of buffer C. Dividing this observed rate by the "ideal rate" indicates the extent to which the activity of His-tagged proteasomes bound to chelating lipid bilayers is preserved. The system mica-bilayer-proteasome was stable during incubation with Suc-LLVY-AMC: upon removal of the mica-supported lipid bilayer with bound proteasomes from the cuvette during hydrolysis, the fluorescence level ceased to rise.

Electron Microscopy—To investigate the interaction of proteasomes with lipid films, 1.5 μg of proteasomes in 15 μl of buffer B were placed in a Teflon well (4 mm diameter, 1 mm deep). The surface of the solution was coated with 1 μl of 1 mM lipid in chloroform/hexane (1:1, v/v). The lipid was, as indicated, SOPC, a mixture of NTA-DODA (no nickel) and SOPC (1:9), a mixture of Ni-NTA-DODA and SOPC (1:9), or a mixture of Ni-NTA-DODA and DSPC (1:9). Following incubation for either 1 h or overnight, the lipid-proteasome assembly was transferred onto a carbon-coated grid by placing the grid onto the droplet for 3 min. Such samples as well as proteasomes adsorbed directly onto carbon-coated grids were stained with 2% uranyl acetate for 30 s and inspected in a transmission electron microscope (CM12, Philips, Eindhoven, The Netherlands) at 120 kV. A Silicon Graphics work station with SEMPER software (18) was used for averaging images using a correlation-based approach (19). An area comprising three unit cells in diameter was chosen as a reference and cross-correlated with the image.

Atomic Force Microscopy—To obtain AFM (atomic force microscope) topographs of the lipid-proteasome assembly, His-tagged proteasomes

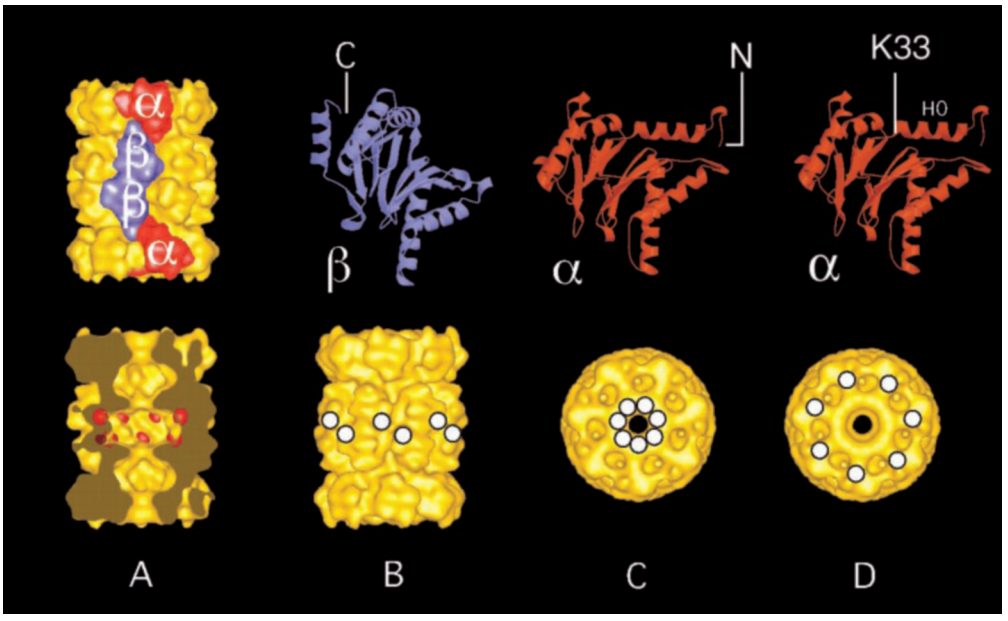

FIG. 1. **Schematic representation of the *T. acidophilum* proteasome showing the three different positions of the His tags.** *A*, low resolution model (~1.2 nm) derived from the atomic coordinates of the *T. acidophilum* proteasome (8). One subunit per heptameric ring is highlighted; α-subunits form the two outer rings, β-subunits form the two inner rings (*top*). The proteasome cut open shows the two entrance channels (one per α-ring) and the central cavity. The N-terminal, proteolytically active threonines are highlighted in *red* (*bottom*). *B*, ribbon drawing of the β-subunit with its C terminus (*top*). Proteasomes His-tagged at the C termini of their β-subunits display His tags around their sides and are referred to as βC-His_6 proteasomes. *White circles* indicate the location of the His tags (*bottom*). *C*, ribbon drawing of the α-subunit with its N terminus (*top*). Proteasomes His-tagged at the N termini of their α-subunits display His tags at their ends around the two cylinder openings and are referred to as αN-His_6 proteasomes (*bottom*). *D*, ribbon drawing of the α-subunit with Lys^{33}. Helix H0 is located between Lys^{33} and the N terminus (*top*). Proteasomes including six or eight consecutive histidines between Lys^{33} and Gly^{34} of their α-subunits display His tags at the ends and are referred to as α turn-His_6 or as α turn-His_8 proteasomes, respectively (*bottom*). Drawings were produced with MOLSCRIPT (49) and RASTER3D (50).

TABLE I
Degradation of casein by proteasomes with and without His-tag (nmol degraded per h and mg of proteasome)

Proteasome	nmol of casein degraded per h and mg of proteasome
Wild-type	170
βC-His_6	177
αN-His_6	93
α turn-His_8	450

were immobilized on supported nickel-chelating lipid bilayers. Between 1 and 5 μg of His-tagged proteasomes in buffer B were adsorbed overnight on the mica-supported bilayer. Care was taken to always keep the solid supported membranes submerged in buffer. After rinsing with buffer B the samples were mounted in the fluid cell of a NANOSCOPE AFM (Digital Instruments, Santa Barbara, CA) and imaged in buffer B either in tapping mode using a drive frequency around 9 kHz and 5–10 nm amplitude of the cantilever, or in contact mode. In either mode, forces exerted by the tip onto the sample were minimized by adjusting the set point manually while scanning. Silicon nitride cantilevers (OMCL-TR400PSA-2, Olympus, Japan) with nominal spring constants of 0.09 newton/m were used; their oxide sharpened tips were cleaned by UV irradiation for ~30 min prior to use.

RESULTS

Proteasomes His-tagged in Various Positions Can be Efficiently Expressed and Purified—The main goal of this study was to immobilize the cylindrical-shaped 20 S proteasome with predetermined orientation, end-on and side-on. To this end, recombinant *T. acidophilum* 20 S proteasomes (referred to simply as "proteasome" in the following) were engineered, carrying His tags at positions favoring one or the other orientation. Proteasomes His-tagged at the sides were obtained by fusing six histidines to the C termini of β-subunits, referred to as βC-His_6 proteasomes (Fig. 1*B*). Proteasomes His-tagged at the ends were obtained by fusing six histidines to the N termini of α-subunits (αN-His_6 proteasomes) (Fig. 1*C*), or alternatively,

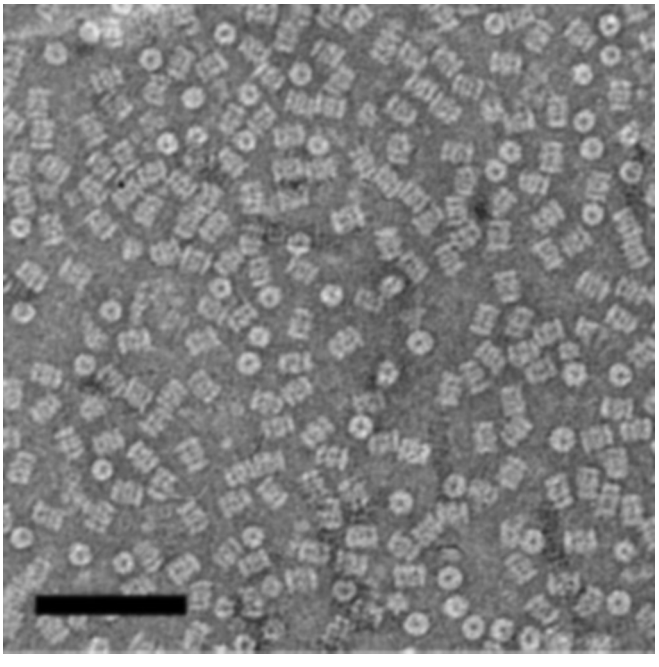

FIG. 2. **Electron micrograph of cylindrical wild-type 20 S proteasomes adsorbed on carbon film.** End-on views appear ring-shaped (11 nm), side-on views appear rectangular (15 nm × 11 nm) with four striations, representing the four proteasomal rings (*scale bar*: 70 nm).

by integrating a stretch of histidines into a solvent-accessible turn of α-subunits connecting helix H0 and strand S1 between Lys^{33} and Gly^{34} (Fig. 1*D*). Proteasomes with six or eight consecutive histidines within this turn are referred to as α turn-His_6 or α turn-His_8 proteasomes, respectively.

Expression levels were similar for all four constructs. βC-

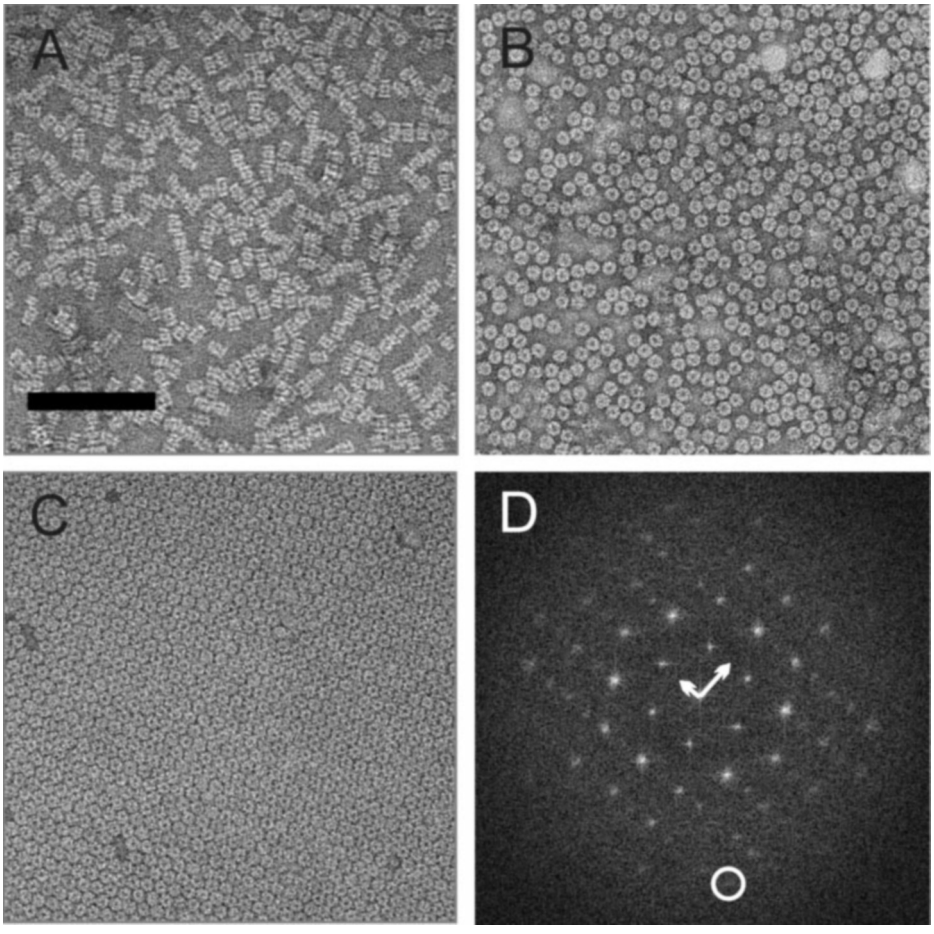

FIG. 3. **According to electron micrographs the orientation of His-tagged proteasomes bound to metal-chelating lipid films depends on the location of the His tags and is highly uniform.** *A*, βC-His_6 proteasomes His-tagged at their sides show exclusively side-on views when adsorbed to nickel-chelating lipid films (*scale bar*, 100 nm in *A–C*). *B*, in contrast, proteasomes His-tagged at their ends uniformly display end-on views when adsorbed to nickel-chelating lipid films, as shown here for α turn-His_8 proteasomes. *C*, αN-His_6 proteasomes His-tagged at their ends form extended, close packed arrays upon overnight incubation with nickel-chelating lipid films. Large two-dimensional crystalline arrays only form with constructs yielding a uniform orientation. *D*, the power spectrum calculated from the two-dimensional crystal in *C*. The two crystallographic vectors are indicated. Reflections go out to 1/2.5 nm^{-1} (indicated by a *white circle*).

His_6, αN-His_6, and α turn-His_8 proteasomes had high affinity for nickel-chelating nitrilotriacetic acid facilitating their efficient purification in a single step on Ni-NTA resin. α turn-His_6 proteasomes, however, could not be purified on Ni-NTA resin, which is indicative of a low affinity for the Ni-NTA group, but could be purified on hydroxyapatite (see "Experimental Procedures").

The Activity of the Proteasome Can Be Both Decreased and Increased—The activity of all constructs with high affinity for Ni-NTA was first assayed using Suc-LLVY-AMC, a standard fluorogenic substrate of the proteasome. Under the experimental conditions chosen (60 °C), hydrolysis of Suc-LLVY-AMC proceeded at rates of 9.5 μmol/h per mg of proteasome for βC-His_6, αN-His_6, and α turn-His_8 proteasomes, close to the rates measured with wild-type proteasomes and in good agreement with previous data (20). Degradation of proteins proceeded at almost identical rates for βC-His_6 and wild-type proteasomes, as judged from hydrolysis of ^{14}C-methylated β-casein (Table I). However, αN-His_6 and α turn-His_8 proteasomes differed in their activities from wild-type proteasomes, indicating that the His tags might affect translocation of long polypeptide chains across the α-ring channel. Interestingly, αN-His_6 proteasomes degraded radiolabeled β-casein at lower rates, whereas α turn-His_8 proteasomes degraded this substrate faster than wild-type proteasomes (Table I).

Proteasomes Can Be Oriented at Metal-chelating Lipid Interfaces via the Location of His Tags—To test whether site-specific binding between His-tagged proteasomes and nickel-chelating interfaces would permit one to control orientation, proteasomes were allowed to interact with nickel-chelating lipid layers. Proteasomes were adsorbed to lipid films containing 10% Ni-NTA-DODA and 90% SOPC or DSPC for either 1 h or overnight. The lipid films were then transferred onto carbon grids and examined by transmission electron microscopy.

In standard transmission electron microscopy preparations where 20 S proteasomes from *T. acidophilum* are applied to carbon film, they show up in two characteristic orientations (21): ring-shaped end-on views with a diameter of 11 nm and rectangular side-on views (15 nm × 11 nm) with a characteristic pattern of four striations, representing the four proteasomal rings; a typical example is seen in Fig. 2. Likewise, when adsorbed unspecifically to SOPC lipid films, proteasomes are seen randomly oriented, regardless of the presence of His tags.

In contrast, the orientation of isolated, His-tagged proteasomes bound to metal-chelating lipid films was highly uniform and in line with expectations: βC-His_6 proteasomes His-tagged at their sides displayed exclusively side-on views (Fig. 3*A*), whereas αN-His_6 and α turn-His_8 proteasomes His-tagged at their ends displayed exclusively end-on views (Fig. 3*B*). α turn-His_6 proteasomes adsorbed randomly oriented, which is not surprising given their low affinity for Ni-NTA resin.

All components of the His tag-nickel-NTA system are required to achieve uniform orientation. In fact, proteasomes were randomly oriented if (i) wild-type proteasomes lacking His tags were adsorbed on Ni-NTA-DODA/SOPC (1:9), (ii) His-tagged proteasomes were adsorbed (in the presence of nickel ions) on SOPC films lacking NTA-DODA, or (iii) His-tagged proteasomes were adsorbed on NTA-DODA/SOPC (1:9) in the absence of nickel ions (in the presence of EDTA). The strict dependence of orientation on all components of the His tag-nickel-NTA system confirms that binding of His-tagged proteasomes to metal-chelating lipid interfaces is specific.

The Activity of Proteasomes Bound to Metal-chelating Lipid

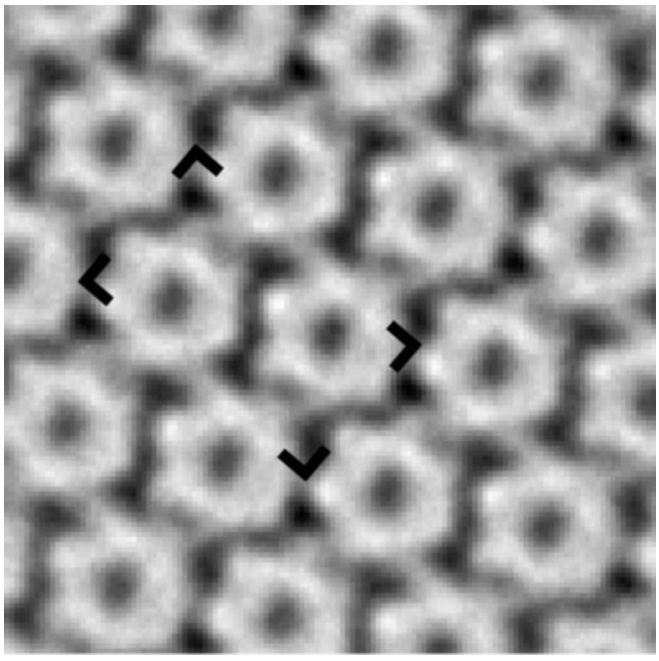

FIG. 4. **Correlation average of the two-dimensional crystal with αN-His$_6$ proteasomes (see Fig. 3*C*) indicating pg symmetry.** The unit cell *outlined by brackets* measures 19.5 × 11.2 nm. Within *rows running diagonally* from the *left bottom* to the *right top*, proteasomes interlock with their neighbors.

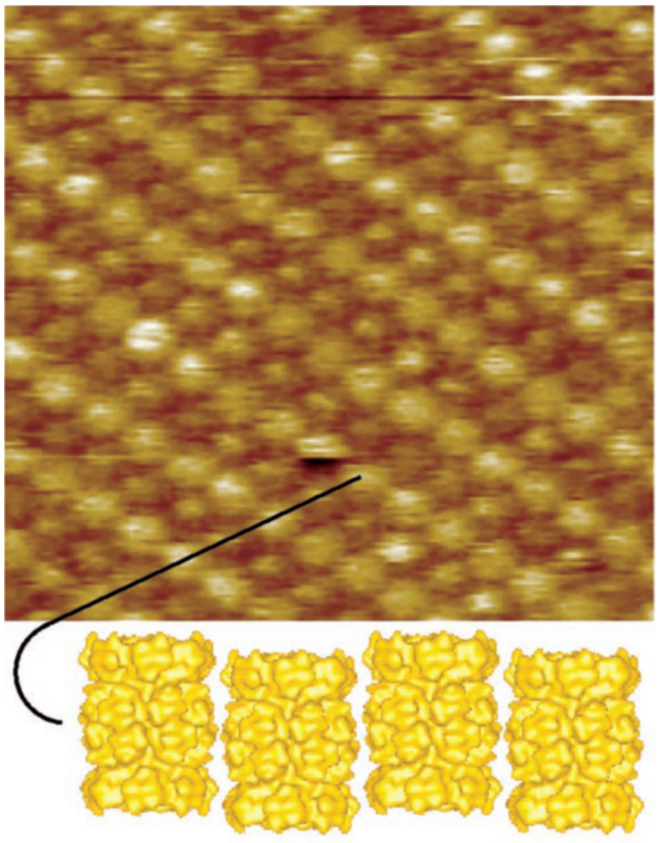

FIG. 5. **AFM topograph showing a crystal of αN-His$_6$ proteasomes.** Proteasomes within crystals are arranged at 2 levels; rows of proteasomes *running diagonally* from the *left top* to the *right bottom* alternate in distance from the support by about 2 nm. The *cartoon* at the *bottom* illustrates the staggered arrangement of proteasomes along the drawn *line*. Neighboring proteasomes nest ring-to-waist into each other by up and down shifts along the proteasomal cylinder axis. The picture was taken in contact mode (software zoom, 150 × 150 nm; scan area, 400 × 400 nm).

Interfaces Is Well Preserved—To demonstrate that immobilization of His-tagged proteins at metal-chelating lipid interfaces is biocompatible, the activity of immobilized proteasomes was compared with the activity of proteasomes in solution. One set of measurements was performed at 60 °C with the βC-His$_6$ and the αN-His$_6$ mutants bound directly on vesicles formed by nickel-chelating lipid bilayers (Ni-NTA-DODA/SOPC, 1:9). By this immobilization, activity of the proteasomes was reduced by about 8% for both mutants in comparison to their activity in solution.

Additionally, proteasome activity was measured for βC-His$_6$ proteasomes bound to a mica-supported bilayer. First the activity of a known amount of these proteasomes in solution was assayed. At the suboptimal temperature of 40 °C, which ensured stability of the complete mica-lipid bilayer-proteasome system, hydrolysis of Suc-LLVY-AMC by 300 ng of proteasomes proceeded at a rate of 0.89 nmol/h, which corresponds to 2.97 μmol/h/mg of proteasome.

An equal amount of proteasomes was adsorbed onto a supported nickel-chelating lipid bilayer (Ni-NTA-DODA/SOPC, 1:9) overnight to allow them to bind. Beforehand, the presence of a continuous lipid bilayer was routinely confirmed by AFM. Proteasomes that did not bind to the bilayer released AMC at a rate of 0.2 nmol/h. Subtracting this rate from the rate at which 300 ng of proteasomes in solution released AMC equals the rate at which those proteasomes bound to the bilayer would release AMC if their activity was not affected by immobilization at all: 0.69 nmol/h (the ideal rate). The rate at which the proteasomes immobilized on the supported bilayer overnight actually released AMC was measured to be 0.35 nmol/h, which amounts to 51% of the ideal rate.

Oriented, His-tagged Proteasomes Crystallize in Two Dimensions on Fluid Metal-chelating Lipid Films—Proteasomes bound to fluid nickel-chelating lipid films end-on (αN-His$_6$ and α turn-His$_8$) showed a high propensity to self-organize in two dimensions. Small close packed arrays of proteasomes were already observed after incubation for 1 h with Ni-NTA-DODA/SOPC (1:9) films. Much larger arrays were observed after overnight incubation (*e.g.* Fig. 3*C*). Under the same conditions, βC-His$_6$ proteasomes also formed densely packed protein layers, but only a few small ordered patches were observed. His-tagged proteasomes were also found to orient on nickel-chelating lipid films when SOPC was replaced by DSPC (Ni-NTA-DODA/DSPC, 1:9). However, no two-dimensional organization was observed on such lipid films. Possibly, DSPC restricts the lateral mobility of the lipid-bound proteasomes.

Power spectra calculated from negatively stained two-dimensional arrays of αN-His$_6$ proteasomes indicated that the organization of proteasomes within the two-dimensional arrays went beyond simple close packing and showed diffraction spots to 1/2.5 nm^{-1} (Fig. 3*D*). Correlation averaging revealed that the rotation of proteasomes about their 7-fold symmetry axis is limited to discrete angles (Fig. 4), giving rise to crystals of pg symmetry.

Images of the two-dimensional crystals of αN-His$_6$ proteasomes on supported nickel-chelating lipid bilayers were also taken by AFM (Fig. 5). Crystals could be repeatedly scanned without apparent degradation. AFM topographs revealed that αN-His$_6$ proteasomes alternated in height within the crystals; every second row of proteasomes stood out by about 2 nm, adding a doubled period to the close packing (Fig. 5). This pattern of alternating rows was continuous throughout scan areas as large as 2 × 2 μm. The diameter of αN-His$_6$ proteasomes in the two-dimensional crystals was 11 nm with their ends appearing dome-shaped in AFM topographs. Possibly, the central channel in α-rings was not visible because of the pres-

ence of seven His tags per α-ring. The appearance of different proteasomes was slightly heterogeneous, the arrangement of the seven His tags may vary for different proteasomes. However, the appearance of proteasomes did not change in time during repeated scanning.

DISCUSSION

The Orientation of His-tagged Proteins with Respect to Metal-chelating Lipid Interfaces Can Be Controlled via a Judicious Choice of His Tag Position—Recombinant DNA techniques allow one to introduce specific sites of attachment into proteins. Cysteines (22) and, more commonly, amino acid sequences including His tags (1) are used for site-specific immobilization. To demonstrate, however, that site-specific immobilization can lead to uniform orientation it is necessary to vary the location of an affinity site within otherwise identical molecules and to show that thereby their orientation can be changed.

Previously, cysteine residues have been used to manipulate the orientation of proteins on solid supports. To this end, the location of an engineered cysteine has been varied in cytochrome b_5. Two mutants having either Thr^8 or Thr^{65} replaced by cysteine (T8C or T65C) have been shown to differ in their mean orientation with respect to their support upon site-specific immobilization (23, 24). Linear dichroism measurements revealed that the heme group of cytochrome b_5 (T8C) adopted an average angle of 78° with respect to the support, whereas the heme group of cytochrome b_5 (T65C) adopted an average angle of 45° with respect to the support (24). However, the distribution of orientations has been shown to be rather broad when molecules were immobilized via a single cysteine: cytochrome *c* immobilized on a self-assembled monolayer with terminal thiol groups displayed a broad distribution of heme orientations (25), as judged from a combination of fluorescence intensity and polarization measurements (26, 27). Thus, whereas site-specific immobilization will influence orientation, it will not necessarily lead to a uniform orientation.

Taking advantage of the chelating lipid concept (17, 28), the effect of the location of the His tag on the orientation of proteins at a chelating lipid film has been investigated using two variant RNA polymerase I molecules, His-tagged on either subunit AC_{40} or subunit ABC_{23}. Within two-dimensional crystals, orientation was found to correlate with the location of the His tag (29); both variants contacted the lipid film with their respective tagged subunits, thus interacting with the lipid film in reversed orientation to yield different crystal forms. However, isolated polymerase molecules outside the crystal patches appeared in several different orientations. This indicates that the uniform orientation observed within the crystal patches may at least in part result from lateral protein-protein interactions.

To investigate the potential use of the His tag as a handle to exert control over the orientation of a protein, 20 S proteasomes His-tagged at different sites were examined by transmission electron microscopy and AFM after binding to nickel-chelating lipid films. When incubation periods were short enough, proteasomes were mostly well separated from one another; therefore, we can assume that their orientation is determined exclusively by their interaction with the lipid film. Proteasomes His-tagged at their sides (βC-His_6) uniformly displayed side-on views when bound to nickel-chelating lipid films (Fig. 3*A*). Proteasomes His-tagged at their ends (αN-His_6 and α turn-His_8) were bound with their ends to the nickel-chelating lipid film, resulting exclusively in end-on views (Fig. 3*B*).

Interestingly, six histidines are sufficient to control orientation when fused to the C terminus of β-subunits or the N terminus of α-subunits, whereas a stretch of eight histidines are required to control orientation when the His tag is inserted between Lys^{33} and Gly^{34} of α-subunits. Proteasomes having only six consecutive histidines between Lys^{33} and Gly^{34} of their α-subunits were found to be randomly oriented on nickel-chelating lipid films in line with their low affinity for Ni-NTA. Possibly, a stretch of six histidines "pinned" at both ends is not sufficiently accessible or conformationally too restricted to tightly coordinate Ni-NTA. It is interesting to note that isolated histidines on the surface of the β-subunit of the proteasome (His^{109}) have no effect on the orientation, as is evident from the random orientation of wild-type proteasomes when incubated with nickel-chelating lipid films.

Uniform orientation was only achieved when all components of the His tag-nickel-NTA system were present. The lack of any one component resulted in the coexistence of side-on and end-on views. Thus, the uniform orientation is because of specific interactions between His tags and the metal-chelating lipid layer. Both the end-on and the side-on orientation proteasomes are probably bound to chelating lipid films via several His tags. For the end-on orientation, as many as seven His tags might participate in the interaction. This multipoint attachment may play a critical role in turning site-specific binding into oriented immobilization.

Uniform Orientation of His-tagged Proteasomes on Nickel-chelating Lipid Films Promotes Their Two-dimensional Crystallization—Incubation of His-tagged proteasomes with fluid metal-chelating lipid films for longer periods of time often resulted in two-dimensional crystalline arrays (see Fig. 3*C*). When the 20 S proteasomes occurred both in side-on and end-on orientations, as was the case with wild-type proteasomes on SOPC lipid films, only very small crystal patches were observed. Possibly, the nonuniform orientation prevents the growth of larger two-dimensional crystals. With βC-His_6 proteasomes, and more often with αN-His_6 and α turn-His_8 proteasomes, larger crystalline patches were observed. The orientation of the proteasomes in these two-dimensional crystals was the same as found for the corresponding isolated proteasomes. Thus, the uniform orientation achieved with these constructs appears to promote two-dimensional crystallization. The potential of His tags to be used in combination with metal-chelating lipid layers to generate two-dimensional crystalline arrays has been recognized some time ago (17, 29–33). It is seen as a widely applicable and rational strategy to produce two-dimensional crystals of soluble and membrane proteins suitable for electron crystallography.

When crystals formed by αN-His_6 proteasomes were analyzed in more detail, it was found that the close packed proteasomes optimize their packing by a rotation about their 7-fold symmetry axis so as to form rows of interlocking proteasomes. The directionality of interlocking alternates between neighboring rows (Fig. 4). The resulting two-dimensional crystals of pg symmetry are built from a unit cell containing two proteasomes related by glide reflection. The parameters of the unit cell are a = 19.5 nm, b = 11.2 nm, $\gamma = 90°$.

After very long periods of incubation, multilayered structures were occasionally observed. Their formation may be promoted by the fact that bound proteasomes not only display His tags toward the lipid layer, but also in the direction pointing away from it. Other His-tagged molecules may bind to the primary arrays decorated with His tags, possibly mediated by small amounts of nickel released from the Ni-NTA resin during purification.

Binding of His-tagged Proteins to Metal-chelating Lipid Interfaces Is Biocompatible—Although it has been shown for several enzymes that they retain their activity after immobilization (see Refs. 34 and 35), this cannot be taken for granted. Not only the immobilization might affect the activity, also the mere presence of His tags can, in principle, have an influence. There-

fore, it was important to show that the activity of His-tagged proteasomes (βC-His_6, αN-His_6, and α turn-His_8) against Suc-LLVY-AMC in solution was identical to that of wild-type proteasomes. Obviously, the presence of His tags on the proteasomal exterior has no strong effects on peptide hydrolysis.

A critical step in the degradation of proteins is their uptake through the channel formed by the α-rings that controls access to the interior. In the crystal structure of the *T. acidophilum* proteasome this channel appears to be open with a diameter of 1.3 nm (8), in the yeast proteasome it is closed by the interdigitating N-terminal residues of several α-type subunits (36). However, because N-terminal residues 1 to 12 were disordered in the case of the *Thermoplasma* proteasome, it is likely that here too the channel is partially occluded. Interestingly, extending the N termini of the α-subunits by six additional His residues causes a reduction in the rate of protein degradation, suggesting that they impose a further steric hindrance. Conversely, the degradation of radiolabeled β-casein by α turn-His_8 proteasomes was accelerated compared with wild-type proteasomes (Table I). Possibly, a His tag inserted between helix H0 and β-strand S1 of the α-subunits disrupts the contact of helix H0 with the cleft formed by the β-sandwich, relieving the blockage of the α-ring channels by the residues N-terminal to H0, and thus facilitates the uptake of protein substrates.

It has been shown previously that proteasomes immobilized on supported nickel-chelating lipid bilayers via His tags located at the C termini of their α-subunits retain proteolytic activity (37). Surface plasmon resonance measurements allowed the authors of Ref. 37 to monitor the loss of mass from the interface because of dissociation of proteolytic fragments generated from oxidized insulin β-chain by proteasomes. In the experiments described in this article we have measured the activity of immobilized proteasomes by direct observation of the products of hydrolysis. We observed only a small reduction of hydrolytic activity against Suc-LLVY-AMC after immobilization.

Hydrolysis by βC-His_6 proteasomes bound side-on to vesicles at low surface coverage was reduced by 8%. When immobilized on mica-supported bilayers instead, the activity of βC-His_6 proteasomes was reduced by 50%. However, several factors may cause this more pronounced reduction of activity compared with proteasomes bound to vesicles. Whereas in the latter case, surface coverage was only 3%, surface coverage was close to complete for the supported bilayers. Clearly, access to the entrance channels of proteasomes will be partly blocked at such high coverage. Additionally, the substrate concentration at the interface will be different for a flat, extended bilayer and for small vesicles for geometric reasons.

Whereas both entrance/exit channels are obviously accessible in the βC-His_6 proteasomes, this is not the case with αN-His_6 proteasomes in the end-on orientation. One could envisage that the channel directed to the lipid layer is less accessible than the opposite one and a quantification of the activity of proteasomes in this orientation could provide some insight into the functional interplay of both channels. In fact, such measurements show that the activity of the αN-His_6 proteasomes in end-on orientation and at low coverage was reduced by only 8%, the same small reduction as found with βC-His_6 proteasomes bound side-on. This observation is consistent with a scenario in which, at least in the case of small substrates, both substrates and products can pass through the same pore. However, it is also possible that the entrance facing the lipid film is not obstructed sufficiently. Complete sealing of this entrance has to be expected for two-dimensional crystals on lipid films, but the corresponding measurements of activity are very problematic because the percentage of two-dimensional crystals in the preparation cannot be quantified accurately enough. Utilizing the His-tag/Ni-chelator system for analysis of the functional interplay of both channels thus needs more complex investigations.[2]

Supported Chelating Lipid Bilayers Are a Versatile Support for Scanning Probe Microscopy of Proteins—AFM allows one to visualize biological structures in action under near physiological conditions and, in favorable cases, with subnanometer resolution (38). In many cases, closely packed arrays or two-dimensional crystals have been found to facilitate attaining high resolution (39–41). One strategy that has been explored to obtain such arrays is the use of streptavidin films grown on biotinylated lipid films (42) as a matrix for growing oriented arrays of biotinylated proteins (43, 44). However, the self-organization of the underlying two-dimensional crystalline streptavidin matrix imposes severe steric limitations on the two-dimensional arrangement of proteins bound to it and, moreover, these proteins need to be biotinylated in a site-specific manner.

Similar restrictions apply to self-assembled monolayers carrying NTA groups (45); nevertheless, they have been used successfully to monitor the transcription of circular, single-stranded DNA templates by AFM (46). The His tag / metal-chelating lipid layer approach described here has two important advantages. First, proteins are frequently expressed with a His tag in the first instance to facilitate their purification. Second, lipid monolayers are more flexible as a matrix than self-assembled monolayers; they allow one to influence the lateral organization via the phase behavior of the chosen lipid. If desired, a condensed lipid film will keep immobilized molecules separated, whereas a fluid lipid film will allow lateral protein-protein interactions and may thus favor dense arrays or even two-dimensional crystallization.

The αN-His_6 proteasome two-dimensional crystals were found to be well suited for imaging with the AFM. The appearance of the proteasomes in the crystals did not change with time during repeated scanning. Based on AFM recordings, yeast 20 S proteasomes have been reported to switch between 2 distinct conformations (47). In contrast, the AFM images of proteasomes in two-dimensional arrays did not reveal the existence of different conformational states. The AFM images gave insight into the vertical packing of crystalline proteasomes, which cannot be deduced from (two-dimensional) electron micrographs. Proteasomes were found to be arranged in 2 levels in AFM topographs. Proteasomes in one row were elevated with respect to proteasomes in neighboring rows by ~2 nm, half the height of a single proteasomal ring (Fig. 5). Apparently, proteasomes within the two-dimensional crystals optimize their packing not only by interlocking laterally, but also by a vertical shift along their cylinder axis. As a result, one ring of the proteasome fits into its neighbors waist. To pack in that manner, proteasomes have to be able to move away from the interface by 2 nm. Assuming that all proteasomes within a crystal are actually bound to the lipid film requires that their linkage be rather flexible. Possibly, this flexibility can be attributed to the last, disordered N-terminal residues 1–12, to which the His tag is appended in αN-His_6 proteasomes. Such a flexible linker might prove useful in many systems and could similarly be realized in the form of a short stretch of disordered residues leading up to a His tag.

In addition to facilitating high resolution studies, immobilizing proteins in a predetermined orientation will also enable dynamic studies of their interaction with substrates or cofactors in real time. Binding and dissociation of individual GroES cofactors from GroEL chaperonin molecules on a mica support has been followed with the AFM (48). GroEL molecules ori-

[2] S. Hutschenreiter and R. Tampé, manuscript in preparation.

ented spontaneously with one GroES binding face directed toward the AFM tip. However, the orientation of unspecifically adsorbed molecules will often be random or unfavorable. In contrast, the His tag-nickel-NTA system allows one to bind molecules in an orientation conducive to further investigation. For example, the interaction of regulatory particles with proteasomes bound end-on will be readily accessible to an AFM tip as height fluctuations.

Acknowledgments—We gratefully acknowledge E. Seemüller for providing the plasmids coding for wild-type and βC-His_6 proteasomes, E. Seemüller and D. Voges for sharing molecular biology expertise, and M. Boicu for sequencing. We thank C. Zeth for assistance with the rendering software.

REFERENCES

1. Hochuli, E., Bannwarth, W., Döbeli, H., Gentz, R., and Stüber, D. (1988) *Biotechnology* **6,** 1321–1325
2. Hochuli, E., Döbeli, H., and Schacher, A. (1987) *J. Chromatogr.* **411,** 177–184
3. Dietrich, C., Schmitt, L., and Tampé, R. (1995) *Proc. Natl. Acad. Sci. U. S. A.* **92,** 9014–9018
4. Dorn, I. T., Neumeier, K. R., and Tampé, R. (1998) *J. Am. Chem. Soc.* **120,** 2753–2763
5. Coux, O., Tanaka, K., and Goldberg, A. L. (1996) *Annu. Rev. Biochem.* **65,** 801–847
6. Baumeister, W., Walz, J., Zühl, F., and Seemüller, E. (1998) *Cell* **92,** 367–380
7. Voges, D., Zwickl, P., and Baumeister, W. (1999) *Annu. Rev. Biochem.* **68,** 1015–1068
8. Löwe, J., Stock, D., Jap, R., Zwickl, P., Baumeister, W., and Huber, R. (1995) *Science* **268,** 533–539
9. Seemüller, E., Lupas, A., Stock, D., Löwe, J., Huber, R., and Baumeister, W. (1995) *Science* **268,** 579–582
10. Seemüller, E., Lupas, A., and Baumeister, W. (1996) *Nature* **382,** 468–470
11. Wenzel, T., and Baumeister, W. (1995) *Nat. Struct. Biol.* **2,** 199–204
12. Lupas, A., Baumeister, W., and Hofmann, K. (1997) *Trends Biochem. Sci.* **22,** 195–196
13. Zwickl, P., and Baumeister, W. (1999) *Nat. Cell Biol.* **1,** E97–E98
14. Schmidt, M., Lupas, A. N., and Finley, D. (1999) *Curr. Opin. Chem. Biol.* **3,** 584–591
15. Glickman, M. H., Rubin, D. M., Fu, H. Y., Larsen, C. N., Coux, O., Wefes, I., Pfeifer, G., Cejka, Z., Vierstra, R., and Baumeister, W. (1999) *Mol. Biol. Rep.* **26,** 21–28
16. Peters, J. M., Cejka, Z., Harris, J. R., Kleinschmidt, J. A., and Baumeister, W. (1993) *J. Mol. Biol.* **234,** 932–937
17. Schmitt, L., Dietrich, C., and Tampé, R. (1994) *J. Am. Chem. Soc.* **116,** 8485–8491
18. Saxton, W. O., and Baumeister, W. (1979) *Ultramicroscopy* **4,** 343–354
19. Saxton, W. O., and Baumeister, W. (1982) *J. Microsc.* (*Oxf.*) **127,** 127–138
20. Zwickl, P., Ng, D., Woo, K. M., Klenk, H. P., and Goldberg, A. L. (1999) *J. Biol. Chem.* **274,** 26008–26014
21. Dahlmann, B., Kopp, F., Kuehn, L., Niedel, B., Pfeifer, G., Hegerl, R., and Baumeister, W. (1989) *FEBS Lett.* **251,** 125–131
22. Persson, M., Bulow, L., and Mosbach, K. (1990) *FEBS Lett.* **270,** 41–44
23. Stayton, P. S., Olinger, J. M., Jiang, M., Bohn, P. W., and Sligar, S. G. (1992) *J. Am. Chem. Soc.* **114,** 9298–9299
24. Yeung, C., Purves, T., Kloss, A. A., Kuhl, T. L., Sligar, S. G., and Leckbrand, D. (1999) *Langmuir* **15,** 6829–6836
25. Wood, L. L., Cheng, S.-S., Edmiston, P. L., and Saavedra, S. S. (1997) *J. Am. Chem. Soc.* **119,** 571–576
26. Bos, M. A., and Kleijn, J. M. (1995) *Biophys. J.* **68,** 2566–2572
27. Bos, M. A., and Kleijn, J. M. (1995) *Biophys. J.* **68,** 2573–2579
28. Shnek, D. R., Pack, D. W., Sasaki, D. Y., and Arnold, F. H. (1994) *Langmuir* **10,** 2382–2388
29. Bischler, N., Balavoine, F., Milkereit, P., Tschochner, H., Mioskowski, C., and Schultz, P. (1998) *Biophys. J.* **74,** 1522–1532
30. Kubalek, E. W., Grice, S. F. J. L., and Brown, P. O. (1994) *J. Struct. Biol.* **113,** 117–123
31. Barklis, E., McDermott, J., Wilkens, S., Schabtach, E., Schmid, M. F., Fuller, S., Karanjia, S., Love, Z., Jones, R., Rui, Y., Zhao, X., and Thompson, D. (1997) *EMBO J.* **16,** 1199–1213
32. Vénien-Bryan, C., Balavoine, F., Toussaint, B., Mioskowski, C., Hewat, E. A., Helme, B., and Vignais, P. M. (1997) *J. Mol. Biol.* **274,** 687–692
33. Celia, H., Wilson-Kubalek, E., Milligan, R. A., and Teyton, L. (1999) *Proc. Natl. Acad. Sci. U. S. A.* **96,** 5634–5639
34. Iwakura, M., and Kokubu, T. (1993) *J. Biochem.* (*Tokyo*) **114,** 339–343
35. Kashlev, M., Martin, E., Polyakov, A., Severinov, K., Nikiforov, V., and Goldfarb, A. (1993) *Gene* (*Amst.*) **130,** 9–14
36. Groll, M., Ditzel, L., Lowe, J., Stock, D., Bochtler, M., Bartunik, H. D., and Huber, R. (1997) *Nature* **386,** 463–471
37. Dorn, I. T., Eschrich, R., Seemüller, E., Guckenberger, R., and Tampé, R. (1999) *J. Mol. Biol.* **288,** 1027–1036
38. Müller, D. J., Fotiadis, D., Scheuring, S., Müller, S. A., and Engel, A. (1999) *Biophys. J.* **76,** 1101–1111
39. Butt, H. J., Downing, K. H., and Hansma, P. K. (1990) *Biophys. J.* **58,** 1473–1480
40. Yang, J., Tamm, L. K., Tillack, T. W., and Shao, Z. (1993) *J. Mol. Biol.* **229,** 286–290
41. Karrasch, S., Hegerl, R., Hoh, J. H., Baumeister, W., and Engel, A. (1994) *Proc. Natl. Acad. Sci. U. S. A.* **91,** 836–838
42. Scheuring, S., Müller, D. J., Ringler, J. B., Heymann, J. B., and Engel, A. (1999) *J. Microsc.* (*Oxf.*) **193,** 28–35
43. Blankenburg, R., Meller, P., Ringsdorf, H., and Salesse, C. (1989) *Biochemistry* **28,** 8214–8221
44. Darst, S. A., Ahlers, M., Meller, P. H., Kubalek, E. W., Blankenburg, R., Ribi, H. O., Ringsdorf, H., and Kornberg, R. D. (1991) *Biophys. J.* **59,** 387–396
45. Sigal, G. B., Bamdad, C., Barberis, A., Strominger, J., and Whitesides, G. M. (1996) *Anal. Chem.* **68,** 490–497
46. Thomson, N. H., Smith, B. L., Almqvist, N., Schmitt, L., Kashlev, M., Kool, E. T., and Hansma, P. K. (1999) *Biophys. J.* **76,** 1024–1033
47. Osmulski, P. A., and Gaczynska, M. (2000) *J. Biol. Chem.* **275,** 13171–13174
48. Viani, M. B., Pietrasanta, L. I., Thompson, J. B., Chand, A., Gebeshuber, I. C., Kindt, J. H., Richter, M., Hansma, H. G., and Hansma, P. K. (2000) *Nat. Struct. Biol.* **7,** 644–647
49. Kraulis, P. J. (1991) *J. Appl. Crystallogr.* **24,** 946–950
50. Merritt, E. A., and Murphy, M. E. P. (1994) *Acta Crystallogr. Sec. D.* **50,** 869–873